



Experimental and Numerical Studies of a Shield Twin Tunnel Undercrossing the Existing High-Speed Railway Tunnel

Ruizhen Fei · Limin Peng · Chunlei Zhang · Jiqing Zhang · Peng Zhang

Received: 9 May 2022 / Accepted: 6 September 2023 / Published online: 5 October 2023
© The Author(s), under exclusive licence to Springer Nature Switzerland AG 2023

Abstract In order to study the influence of shield tunneling on existing high-speed railway lines. Combined with centrifuge test and three-dimensional numerical simulation, the dynamic response of shield tunnel undercrossing existing high-speed railway tunnel was studied, and the influence of settlement joint and steel pipe pile reinforcement on existing tunnel was analyzed. The results show that: (1) the construction joints of existing tunnels significantly reduce the shielding effect of existing high-speed railway tunnels on the ground; (2) The settlement value of the existing tunnel caused by double-line shield tunnel construction needs to be controlled by steel pipe pile reinforcement to meet the requirements of the specification; (3) The double-line shield tunnel construction has little effect on the internal force of the existing high-speed railway tunnel, and the reinforcement of the high-speed railway tunnel lining meets the stress requirements.

Keywords High-speed railway tunnel · Shield tunnel · Tunnel settlement · Construction joints

1 Introduction

With the gradual development and improvement of urban underground transportation network, the construction of new tunnels underneath existing tunnels was gradually increasing. On the basis of the settlement of ground and foundation, the influence of shield tunnel construction was evaluated. Combined with field monitoring data, the polynomial formula for predicting the depth and shape of asymmetric settlement trough in double-track tunnel was determined (Zhang et al. 2019; Kuszyk and Sieminska-Lewandowska 2021). Shield tunneling in urban areas was easy to cause surface subsidence. Combined with engineering examples, the key construction technology, construction control parameters and matters needing attention in the construction period of shield machine were analyzed (Ngueyen et al. 2021; Huang et al. 2021). Considering that the existing tunnel construction has changed the stress state of the original soil, for the shield tunneling project, the soil was not only affected by the construction disturbance of a single new shield tunnel, but also under the overlapping influence of the existing tunnel and the new tunnel, resulting in the complex and difficult to predict the change of the surface displacement (vertical settlement and horizontal displacement). Therefore, the influence of shield tunneling on the surface displacement has become a key issue in such engineering research (Koukoutas and Sofianos 2015; Chen et al. 2016; Liu et al. 2020; Wang et al. 2018).

R. Fei (✉) · L. Peng
School of Civil Engineering, Central South University,
Changsha 410075, China
e-mail: feiruizhen@crdc.com

R. Fei · C. Zhang · J. Zhang · P. Zhang
China Railway Design Corporation, Tianjin 300142, China

The interaction between tunnel and soil was usually studied by field monitoring, numerical simulation and model test. On-site monitoring of tunnel physical and mechanical behavior by collecting data from sensors (Fang et al. 2015; Gue et al. 2017; Klar et al. 2014), but this method was time consuming, clumsy and occasionally damaging sensors. Numerical simulation of soil properties, subway tunnels, adjacent structures and their interactions (Avgerinos et al. 2017; Chakeri et al. 2011; Liu et al. 2011; Ng et al. 2018; Yin et al. 2018; Zhang and Huang 2014; Pan et al. 2018), although some simplifications were needed in the calculation process, this method was efficient in calculating large-scale engineering problems. Centrifuge tests were performed to analyze tunnels with different depths, but simplified consideration was often given to complex strata or detail structures during tests (Byun et al. 2006; Li et al. 2014; Boonyarak and Ng 2015; Boonsiri and Take-mura 2021; Ng et al. 2013, 2015, 2016, 2018, 2022).

In summary, most of the existing studies focus on the influence of new shield tunnels on existing subway tunnels or only on the influence of shield construction disturbance on surface subsidence, but there were few studies on the influence of high-speed railway tunnels under the combined action of new tunnel disturbance and existing tunnel influence. However, the operation speed of high-speed railway tunnels was as high as 350 km, and the deformation of existing tunnels caused by new tunnel construction may reduce the smoothness and safety of high-speed railway operation. Unlike circular subway tunnels, the section of high-speed railway tunnels was usually horseshoe-shaped, which makes the stress or deformation distribution of lining more complex. The lining of high-speed railway tunnel was constructed by construction joints along the longitudinal direction. In theoretical or numerical analysis, the lining was usually simplified as a continuous structure (Pan et al 2018). This kind of underground continuous beam has the effect of reducing the surface deformation caused by tunnel excavation, which was usually considered as a shielding effect (Ng et al. 2015). However, if the high-speed railway tunnel was simplified as a longitudinal beam, it was unclear how the tunnel construction connection affects its shielding effect during tunnel excavation.

In this paper, the influence of shield tunnel under existing high-speed railway tunnel was studied by centrifuge test and three-dimensional numerical

simulation. The influence of settlement joint on existing structure was studied by scale model test, and the influence of steel pipe pile reinforcement on existing high-speed railway tunnel was considered in the process of numerical calculation. The surface deformation, deformation and stress law of existing tunnel lining in double-tunnel construction were mainly studied, so as to provide reference for tunnel design and construction in the future.

2 Project Profile

2.1 Project Overview

The section of Changsha metro line 3 Gas Trade Avenue Station-Xingsha Avenue Station was arranged along the east–west direction of Kaiyuan west road. The section was constructed by shield method. The shield tunnel passes through the existing high-speed railway tunnel at DK34+856, which was vertical to each other, as shown in Fig. 1.

The high-speed railway tunnel has been put into use. Although the design speed in the tunnel was 350 km, the running speed of the high-speed train was usually 300 km. The existing tunnel lining adopts horseshoe section, the section width was 14.9 m, the height was 12.78 m, and the inverted arch thickness was 0.9 m, as shown in Fig. 2a. The inner diameter of the newly-built shield tunnel was 5.4 m, and the outer diameter was 6.0 m. The lining was made of 0.3 m thick C50 reinforced concrete, as shown in Fig. 2b.

2.2 Geological Condition

The typical soil profile in the study area was shown in Fig. 1. The upper layer was an artificial filling soil layer with a depth of 4.6 m. The underlying soil layer was characterized by silty clay with a depth of 8.1 m, followed by strong weathered argillaceous siltstone with a thickness of 3.5 m. The excavation of a new double shield tunnel underneath the weathered argillaceous siltstone was shown in Fig. 1. According to geological exploration reports, the physical and mechanical properties of each soil layer were listed in Table 1.

Fig. 1 Relative position relationship between existing tunnel and new tunnel: **a** plane position relation; **b** section position relation

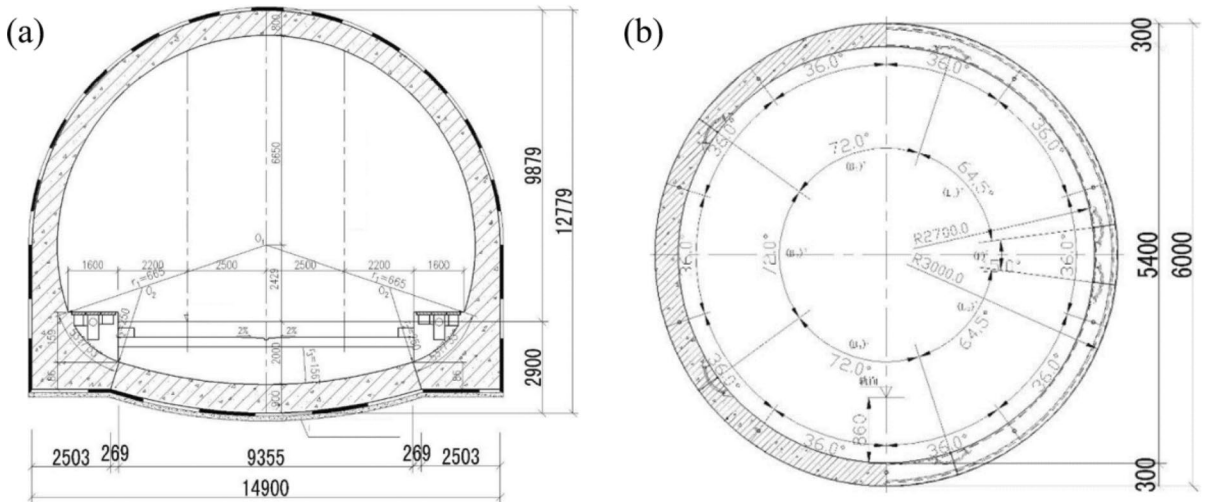
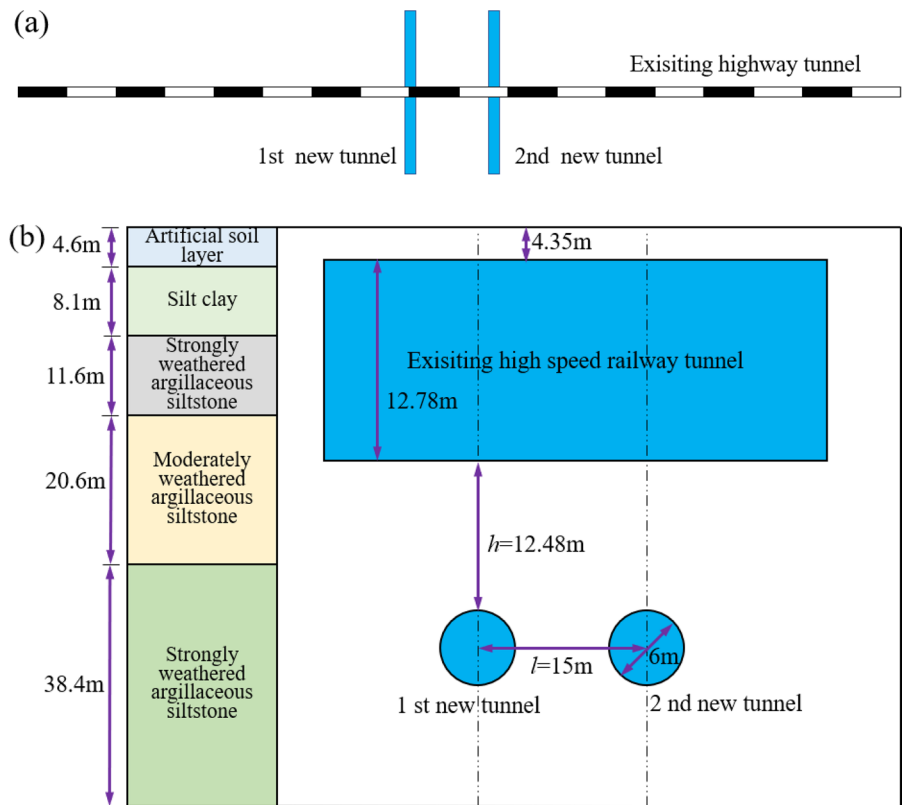


Fig. 2 Tunnel section design: **a** high-speed railway tunnel design section; **b** design section of shield tunnel

Table 1 Physical and mechanical properties of soil layers

Stratum	Soil unit weight (kN/m ³)	Young modulus (MPa)	Inter friction angle (°)	Cohesive stress (kPa)	Poisson ratio
Artificial soil layer	19.6	10	15.0	35	0.35
Silty clay	20.0	30	16.5	42	0.31
Strongly weathered argillaceous siltstone	22.4	400	17.2	50	0.27
Moderately weathered argillaceous siltstone	23.0	1000	20.0	80	0.25

3 Centrifuge Model Tests

3.1 Experimental Device

In this study, two centrifuge model tests were carried out in the centrifuge test device of Hong Kong Polytechnic University. The centrifuge capacity was 400 g-t, and the rotation radius was 4.2 m. These two centrifuge tests were carried out under 60 g (gravity acceleration). The model container used in the test was 1250 mm long, 930 mm wide, and 850 mm high. Except that in test 2, a settlement joint was set on the existing tunnel, the structures of the two tests were completely the same. Figure 3a shows the typical plane diagram of the centrifuge model. The new shield tunnel was vertical to the existing tunnel, and the left tunnel was excavated first, and the right tunnel was excavated later.

Figure 3b shows the typical elevation view of the centrifuge model. The thickness of sand was 800 mm, equivalent to 48 m of the prototype. The buried depths of the built tunnel and the newly excavated tunnel were 72.5 mm and 477.5 mm, respectively, corresponding to 4.35 m and 28.65 m in the field. The section heights of the existing tunnel and the newly excavated tunnel were 184.6 mm and 100 mm, respectively, corresponding to 11.1 m and 6 m on site.

3.2 Tunnel Settlement Joint Model

Figure 4 shows the process of preparing the settlement joint in test 2. The existing tunnel was completely cut off at the middle line. Before the experiment, the two tunnels were temporarily connected by four thin aluminum sheets to facilitate putting them into the model box. Four potentiometers were

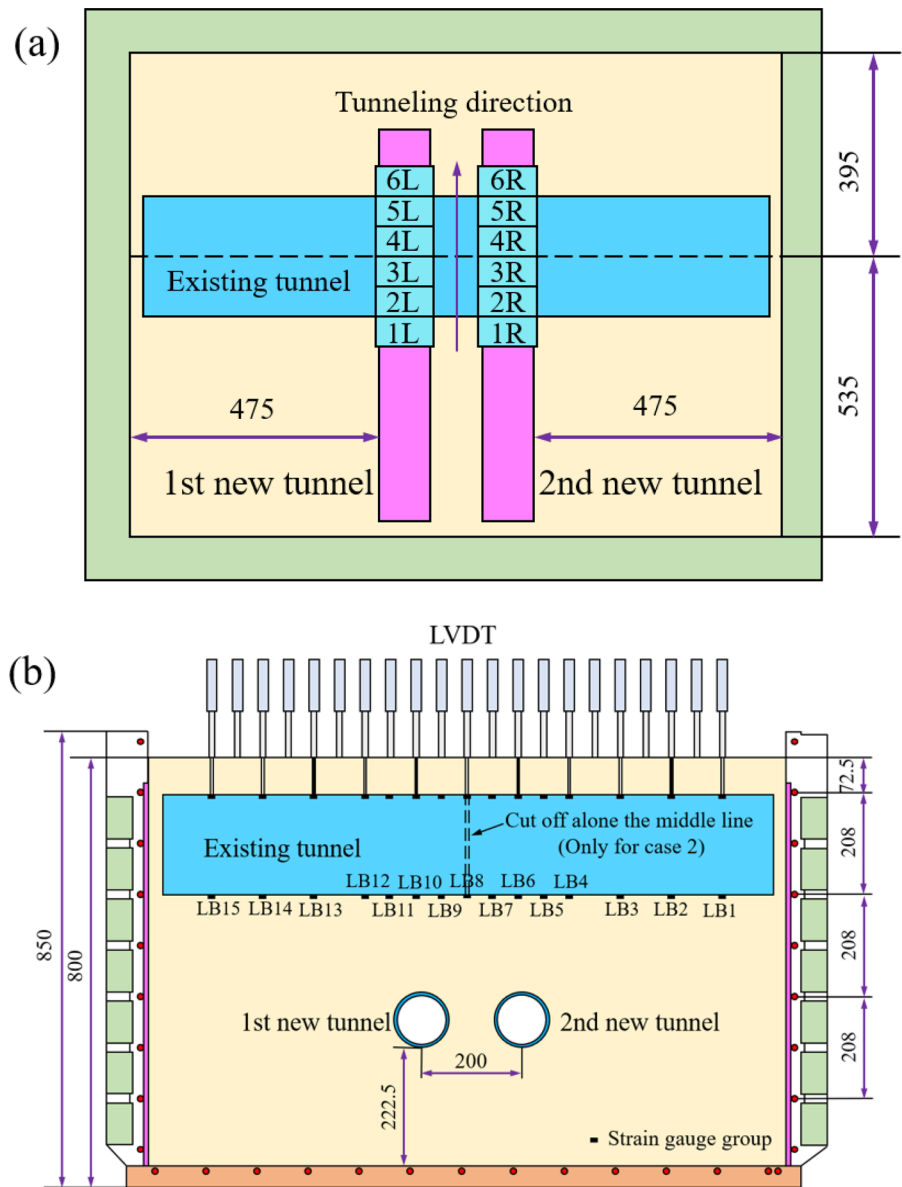
arranged at the middle line position of the internal section of the existing tunnel to measure the change of the inner diameter of the existing tunnel in the vertical and horizontal directions.

3.3 Simulation of Tunnel Excavation

In the actual construction process, shield tunnel construction was composed of earthwork excavation, tunnel lining installation and tail hole grouting. All these construction activities cause surface subsidence, but it cannot distinguish the contribution of each process to surface subsidence and existing tunnel deformation. Therefore, the overall tunnel volume loss was simulated in centrifuge test rather than detailed construction activities. In this study, in general, the simulation method of tunnel volume loss was realized by discharging a large amount of heavy liquid during the construction process, which was a common tunnel excavation simulation technology in the literature. Although this simulation technology cannot capture all tunnel construction activities, the key influence of volume loss was well captured.

As shown in Fig. 5, the model tunnel was composed of rubber bag, dumbbell-shaped frame and six drainage holes. The outer diameter and arm thickness of the rubber film were 100 mm and 1 mm, respectively. This rubber was sealed at both ends of the dumbbell-shaped frame. Two holes were designed at both ends of the dumbbell-shaped frame to remove any bubbles in the model tunnel. The two holes were sealed after removing the bubbles in the model tunnel. The rubber belt was filled with zinc chloride solution. The solution was approximately incompressible, and the density was close to that of sand in the test. In centrifuge test, the simulation of tunnel excavation

Fig. 3 Typical plan and elevation view of centrifuge model: **a** plan view; **b** elevation view



was realized by releasing zinc chloride solution in one rubber bag inside and outside the tunnel lining. By releasing the solution outside the tunnel lining, the ground loss caused by tunnel excavation can be simulated (2%). The self-weight loss in tunnel can be simulated by releasing the solution in tunnel lining. Ng conducted a three-dimensional centrifuge test on the interaction between two tunnels, and found that the weight loss of the tunnel response caused by the excavation below the tunnel was negligible (Ng et al 2013). For convenience, tunnel volume loss was simulated by drainage during construction.

3.4 Test Process

For the sake of simplicity, two centrifugal tests were carried out with dry Toyoura sand with good engineering properties. This was a kind of fine sand with poor gradation, and the particle size (D_{50}) was 0.17 mm. The maximum void ratio (e_{max}), minimum void ratio (e_{min}), specific gravity (G_s) and internal friction angle (φ'_c) were 0.977, 0.597, 2.65 and 31° , respectively. (Ishihara 1993; Shi et al. 2019a, b). Quartz is the main mineral of Toyoura sand, which is crushed under high pressure (higher than 4000 kPa).

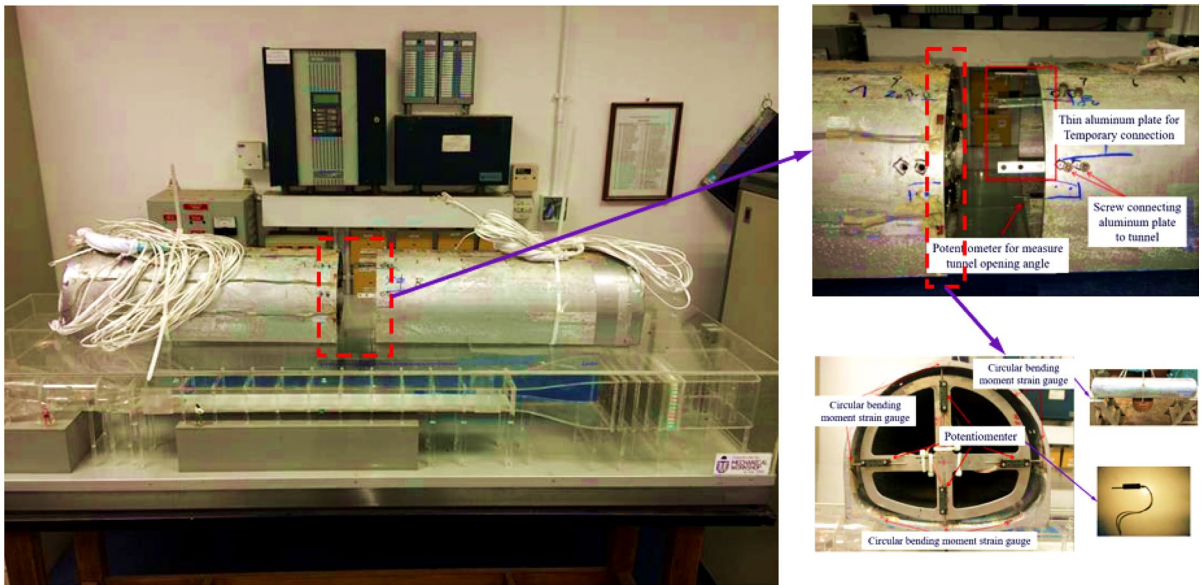


Fig. 4 Preparation process of the settlement joint

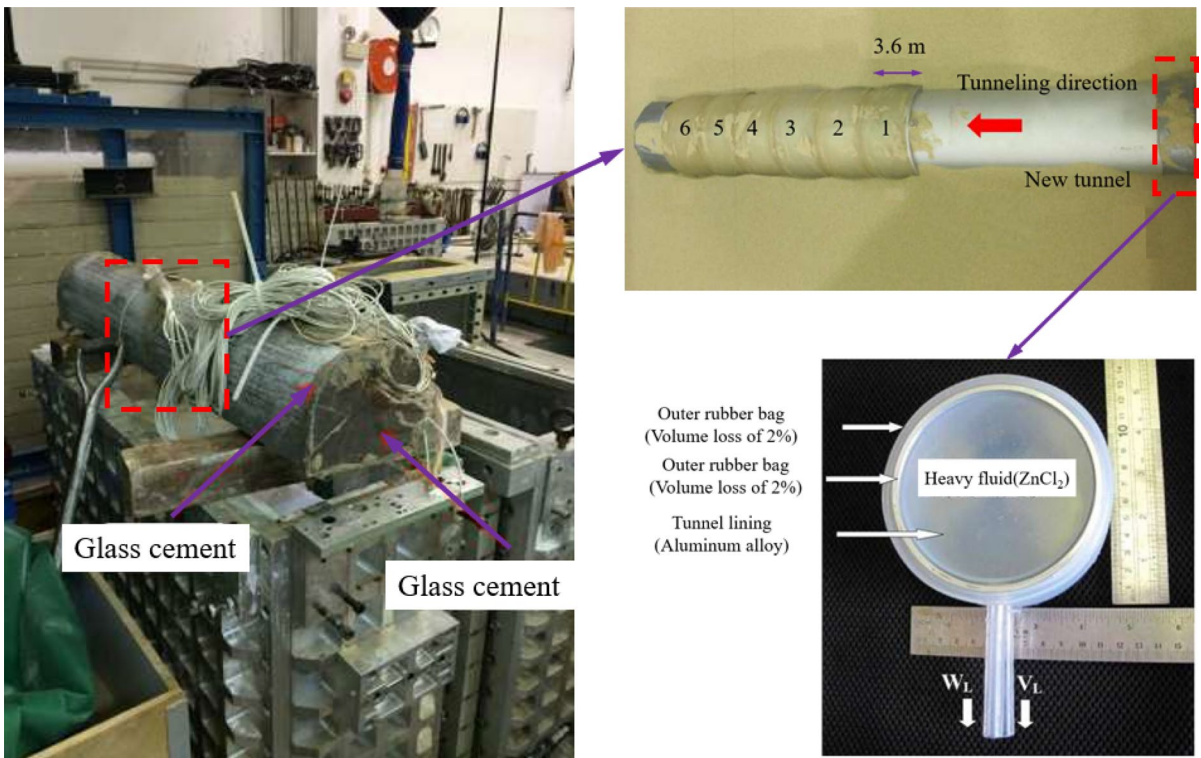


Fig. 5 Simulation system test diagram of formation loss

Therefore, it is not necessary to consider the change of sand properties caused by crushed sand particles. The centrifuge test places a reduced size geotechnical model in a high-speed rotating centrifuge, allowing the geotechnical model to withstand centrifugal acceleration greater than gravity acceleration, in order to compensate for the weight loss of the geotechnical model caused by model scaling. Based on centrifuge testing, we can replace a strongly weathered siltstone layer with a sand layer used in the centrifuge model to investigate the effect of twin tunnels on the existing tunnel and surface settlement.

In this study, sand rain method was used to prepare relatively uniform and repeatable sand samples. In order to obtain medium density sand samples, the measured rainfall distance from the sand surface was maintained at 800 mm. When the sand reaches the inverted arch level of tunnel and pipeline (see Fig. 4), the model tunnels and pipelines were installed respectively. After the model preparation, the average dry densities of sand samples were 1490 and 1493 kg/m³, respectively. The relative densities (D_r) of test 1 (continuous tunnel) and test 2 (joint tunnel) were 0.52 and 0.53, respectively. When sand is spread to 222.5 mm from the bottom of the model box, the new tunnel is parallel with the sand plane to the designed spacing, after the placement of the model, the sand is spread to the height of the existing tunnel (Fig. 6).

3.5 Centrifuge Testing Procedures

After the centrifugal model was prepared, the gravity acceleration gradually increased from 1 to 60 g. When all LVDT and strain gauge readings were stable, the tunnel excavation in the air was simulated by controlling well-drained water. The test was divided into five stages: the centrifuge acceleration rises to 60 g, after the measurement data reading was stable,

the air valve was opened, and the liquid in the water belt was gradually released to simulate the tunneling process of the tunnel. After the zinc chloride solution in each water-saving bag was released, wait for 2 min and release the next section. As shown in Fig. 3a. The excavation process of the newly excavated tunnel was simulated by the method of discharging heavy liquid. The excavation sequence was 1L → 2L → 3L → 4L → 5L → 6L → 1R → 2R → 3R → 4R → 5R → 6R, where 3L, 4L, 3R and 4R were directly below the constructed tunnel. In the test, the excavation length of each section was 60 mm, and the corresponding site was 3.6 m. The lower side of the model box was a reserved square slot for placing the control valves and heavy liquid storage tanks necessary to simulate tunnel excavation.

4 Numerical Analysis

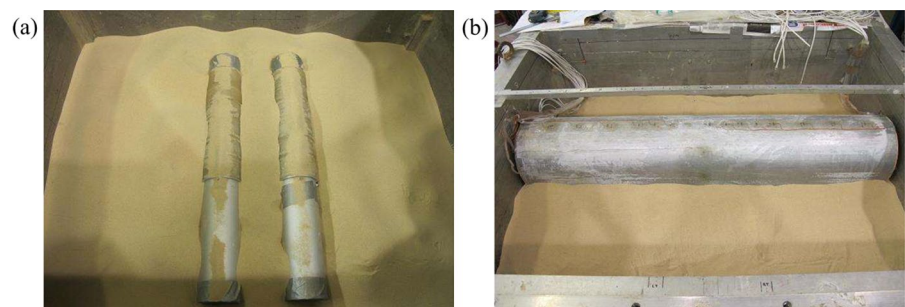
4.1 Model Overview

To further study the influence of settlement joints and steel pipe pile on existing tunnels. The finite element software MADIS/GTS was used to establish a three-dimensional numerical calculation model. The constitutive model was based on the Mohr Coulomb criterion. In 1773, Coulomb proposed a soil pressure theory of soil or rock failure, which was expressed by

$$\tau = c - \sigma \tan \phi,$$

where τ and σ were respectively the shear strength and the normal stress (tensile stress was positive) in the shearing surface; c and ϕ were the cohesion and the angle of internal friction of soil or rock, respectively.

Fig. 6 Preparation process of model box: **a** the sand layer reaches new tunnel; **b** the sand layer reaches existing tunnel



Later, Mohr developed the Coulomb failure condition into the law of shear failure, namely the Mohr–Coulomb criterion, that could be described in terms of the principal stresses ($\sigma_1 \geq \sigma_2 \geq \sigma_3$) as.

$$F = (\sigma_1 - \sigma_3) + (\sigma_1 + \sigma_3) \sin\theta - 2c \cos\theta = 0.$$

A large number of experiments have shown that the M–C criterion was able to reasonably depict the yield or failure behavior of soil and rock.

The size of the three-dimensional numerical calculation model was 120 m × 120 m × 80 m. The grid of the existing tunnel and the new tunnel was locally encrypted. The bottom of the model was completely constrained and the side was horizontally constrained. Three deformation joints were set along the longitudinal direction of the existing high-speed railway tunnel. All deformation joints were filled with entities to restrict their longitudinal displacement. The buried depth of the existing high-speed railway tunnel was 4.3 m, and the tunnel structure was horseshoe section. The buried depth of the new tunnel was 29.6 m. The overall grid of the model was shown in Fig. 7a. The position relationship between the existing tunnel and the new tunnel was shown in Fig. 7b. The reinforced steel pipe pile was shown in Fig. 7c.

4.2 Calculation Conditions

The initial support of the existing high-speed railway tunnel was C35 concrete with a thickness of 35 cm, and the secondary lining was C40 concrete with a thickness of 40 cm. The newly-built shield tunnel adopts C50 concrete with segment diameter of 6 m and thickness of 30 cm. The lining of the existing tunnel, the segments of the new tunnel and the soil were

Table 2 Material properties of the structures

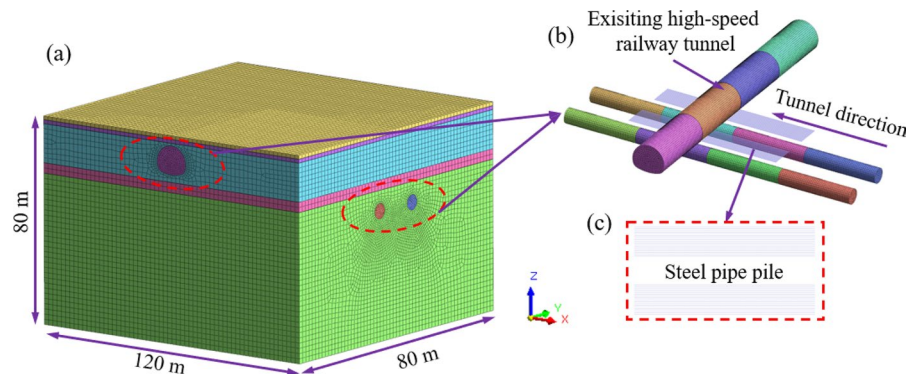
Materials	Unit weight (kN/m ³)	Elastic modulus (MPa)	Poisson ratio
Secondary lining of high speed railway tunnel	25	3.15×10^4	0.20
Invert filling concrete	25	2.56×10^4	0.20
Concrete slab	25	3.25×10^4	0.20
Segment lining	25	2.78×10^4	0.20
Shield machine	78.5	2.10×10^5	0.26

simulated by solid element, and obey the Mohr–Coulomb yield criterion. Considering the influence of segment joint on lining strength, the elastic modulus of segment should be reduced by 20%. The structural physical parameters were shown in Table 2.

4.3 Simulation of Construction Process

Due to the long distance of shield propulsion, alternate passivation of tunnel soil unit and activation of shield shell unit, segment unit and grouting layer were adopted to simulate the process of tunnel excavation and grouting reinforcement. The shield shell, grouting and other layers were simulated by plate element, and the grouting pressure was added at the same time. The cutting effect between the cutterhead and the soil was simulated by applying circumferential force on the soil surface. The simulation of excavation process mainly includes shield excavation, the application of earth pressure, torque, top thrust and grouting reinforcement. Considering that grouting reinforcement needs a process to form strength bearing, the grouting pressure and grouting layer were applied to simulate,

Fig. 7 Finite element calculation model: **a** overall calculation model; **b** the position relationship between the existing tunnel and the new tunnel; **c** steel pipe pile



and the segments were continuously applied with the advancement of shield machines.

In the whole excavation process, the main role of the shield was to support the surrounding soil, passive shield was the shield tail away from the current position; the soil in the passive excavation area was excavated in the actual excavation process; activation segment was the segment assembly in the actual tunneling process; activation grouting was the shield tail grouting in the actual tunneling process, but the grouting has a curing process. Therefore, in the simulation construction process, after all the excavation was completed, the grouting layer was solidified and realized by changing the material properties. The simulation of shield tunneling process was shown in Fig. 8.

5 Results and Discuss

5.1 Deformation Law of Shield Tunneling Under Existing Tunnel

Figure 9 was the vertical displacement nephogram of the existing tunnel when the double-line shield tunnel excavation was completed. It can be seen from Fig. 5 that after the excavation of the left tunnel, the maximum settlement value of the existing tunnel lining appears above the axis of the left tunnel, which was 1.73 mm; after the completion of the right line tunnel excavation, the settlement value distribution of the existing tunnel lining was small at both ends and large in the middle, and the maximum value was 2.56 mm. The settlement value of the existing tunnel caused by the first shield tunnel construction has reached 67% of the completion of the tunnel construction. It can be seen that the first shield tunnel has a great influence.

Fig. 8 Simulation of shield tunneling process

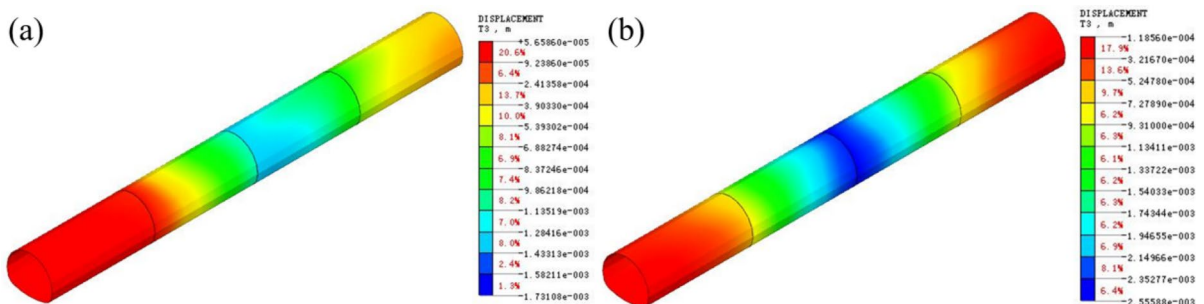
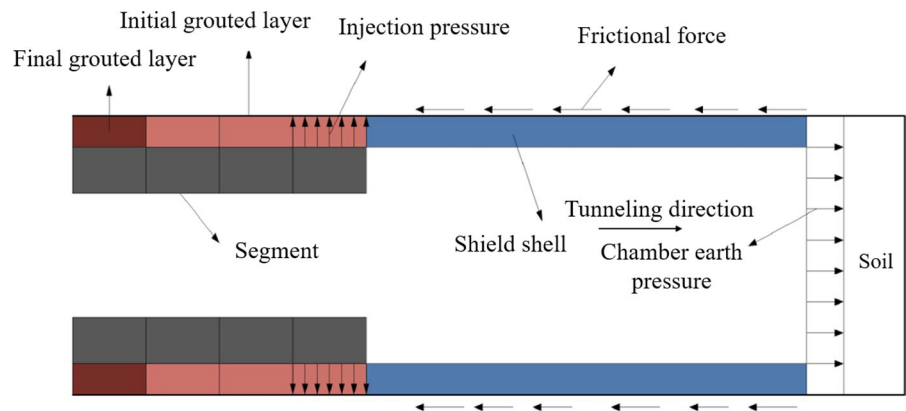


Fig. 9 Horizontal displacement changes of Liuyang River tunnel in different construction stages: **a** after excavation of 1st new tunnel; **b** after excavation of 2nd new tunnel

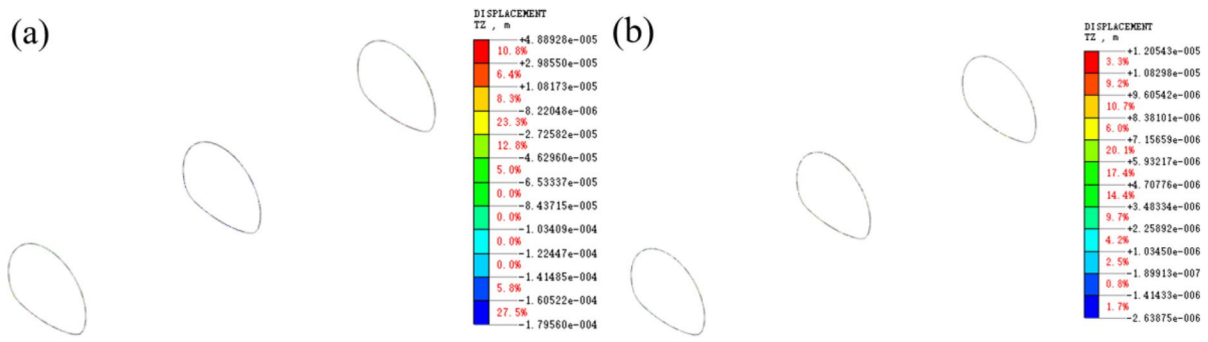


Fig. 10 Construction of Liuyang River tunnel construction seam change figure: **a** after excavation of 1st new tunnel; **b** after excavation of 2nd new tunnel

In addition, shield tunnel excavation has a great influence on the lining of high-speed railway tunnel just above.

Figure 10 was the vertical displacement nephogram of the construction gap when the double-line shield tunnel excavation was completed. It can be seen from the figure that there was no obvious differential settlement between the lining deformation joints. The differential settlements at the three deformation joints from left to right were 0.025 mm, 0.016 mm and 0.023 mm, respectively. After steel pipe pile reinforcement, the differential settlements at the three deformation joints from left to right were 0.009 mm,

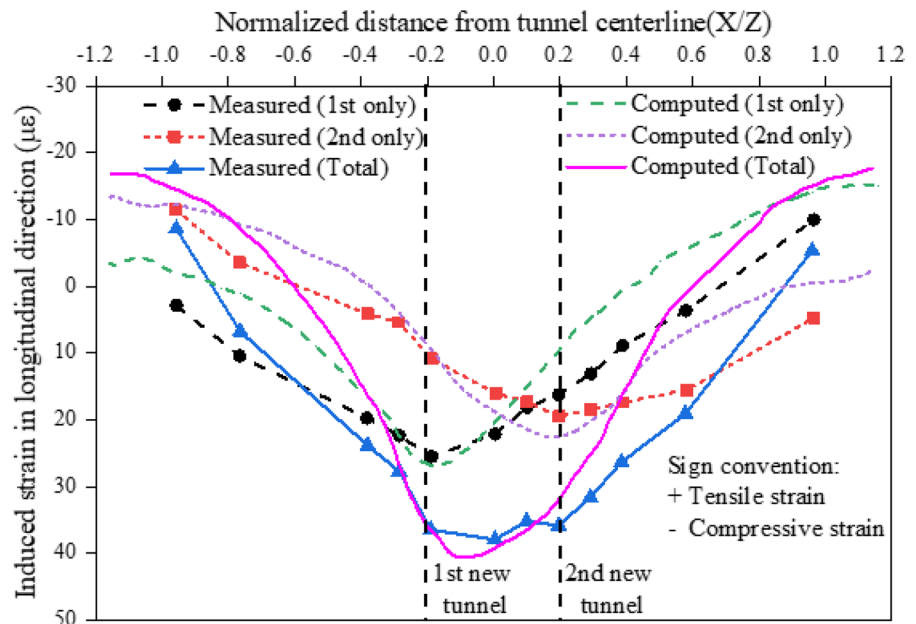
0.006 mm and 0.008 mm. This shows that the reinforcement of steel pipe piles effectively controls the deformation of settlement joints.

Figure 10 shows the longitudinal impact range on the existing high-speed railway Liuyang River Tunnel is about 60 m.

5.2 Longitudinal Bending Strain of Existing Tunnels Induced by Double Tunnel Excavation

Figure 11 shows the bending strain of the existing tunnel arch bottom caused by the double-track shield excavation. It can be seen from the diagram that the

Fig. 11 Influence of double tunnel construction on longitudinal bending moment of existing tunnel



calculated value and the measured value were slightly different, which may be due to the assumption that the existing tunnel was calculated according to the theory of the beam, resulting in inaccurate. However, the calculated values of longitudinal bending strain were in good agreement with the measured values, and the maximum values were basically the same.

As shown in Fig. 11, the bending positive strain occurs on both sides of the middle line of the existing tunnel, and the bending negative strain was at both ends of the existing tunnel. The change was basically consistent with the settlement curve of the arch bottom. After the left and right line shield excavation was completed, the total bending strain in the middle of the existing tunnel was $37.6 \mu\epsilon$, and the negative strains at both ends were $-9 \mu\epsilon$ and $-5 \mu\epsilon$, respectively. Considering that in ACI2001, the ultimate tensile strain (cracking) of unreinforced concrete was $150 \mu\epsilon$. In this test, the measured tensile strain was less than $150 \mu\epsilon$, because the size and thickness of the existing tunnel was very large, resulting in a more

general tunnel (the left and right lines in this test) stiffness was much larger.

The maximum bending strain caused by the excavation of the left line was $25.2 \mu\epsilon$, which appears on the axis of the left line and gradually changes to $-8 \mu\epsilon$. The maximum bending strain caused by right line excavation was 11% smaller than that caused by left line excavation. The arch bottom settlement and longitudinal bending strain results of the existing line caused by the above double-line excavation mean that the influence of the right line of subsequent excavation on the existing tunnel was smaller, which was basically 5–11% smaller. The reason for this phenomenon was that after the left-line shield excavation was completed, the soil stress near the existing tunnel was redistributed. The first excavated left line reduces the soil stiffness in a small range near the excavated tunnel, because the constraint pressure near the tunnel was reduced. However, the stiffness of the adjacent soil was improved due to the increase of the constraint pressure, such as the soil near the existing tunnel and

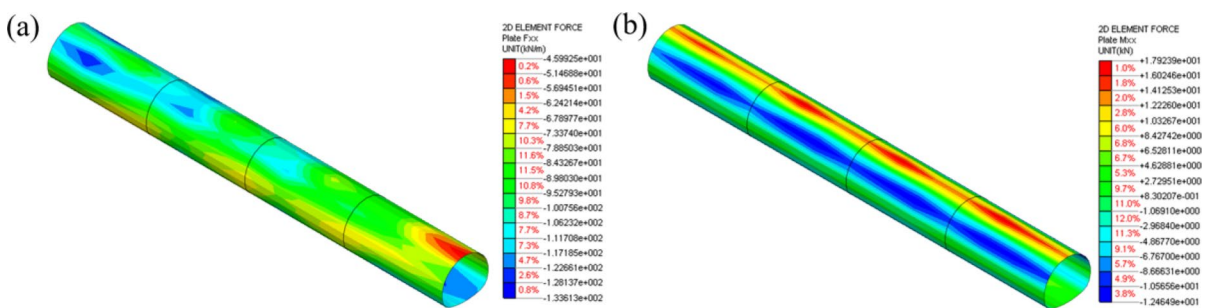


Fig. 12 Internal force diagram of existing tunnel before shield construction: **a** axial force diagram; **b** moment diagram

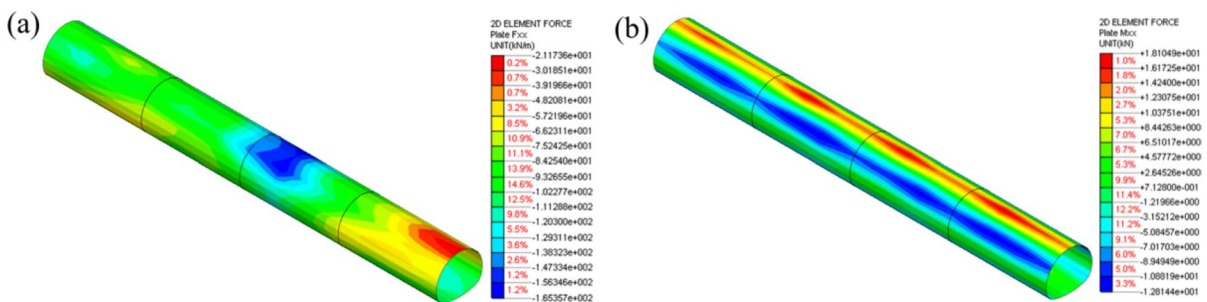


Fig. 13 The internal force diagram of the existing tunnel after the completion of the right line excavation: **a** axial force diagram; **b** moment diagram

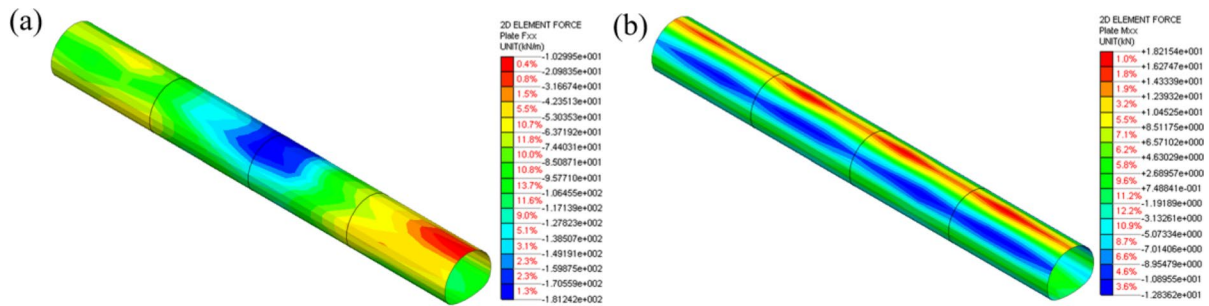


Fig. 14 The internal force diagram of the existing tunnel after the completion of the left line excavation: **a** axial force diagram; **b** moment diagram

the subsequent excavation of the right-line tunnel, so the influence of the right-line excavation on the existing tunnel was smaller. According to Fig. 11, experimental results obtained from the centrifuge model and results with MADIS/GTS software can be mutually verified.

5.3 Internal Force Law of Shield Tunnel Undercrossing Existing Tunnel

Figures 12, 13 and 14 show the internal force contours of the lining of the high-speed railway tunnel before shield construction, after the completion of the right line excavation and after the completion of the left line excavation. It can be seen from the figure that after the lining construction of the existing high-speed railway tunnel was completed, the lining axial force was concentrated at the bottom of the lining and the arch waist position, and the maximum axial force was 1336.1 kN. After the excavation of the right line of the shield, the axial force of the lining of the high-speed railway tunnel above the right line was concentrated at the vault, and the maximum stress concentration was 1653.6 kN; after the excavation of the left line of the shield, the axial force concentration area of the lining extends to the lining just above the left line. The axial force concentration area was located at the deformation joint of the lining, and the maximum axial force was 1812.4 kN, increasing by about 476.3 kN. The comparative analysis shows that shield excavation has a certain influence on the axial force change at the deformation joint of Liuyang River tunnel lining, and the increase was small, which was far less than the allowable bearing capacity of high-speed railway tunnel. According to the variation of

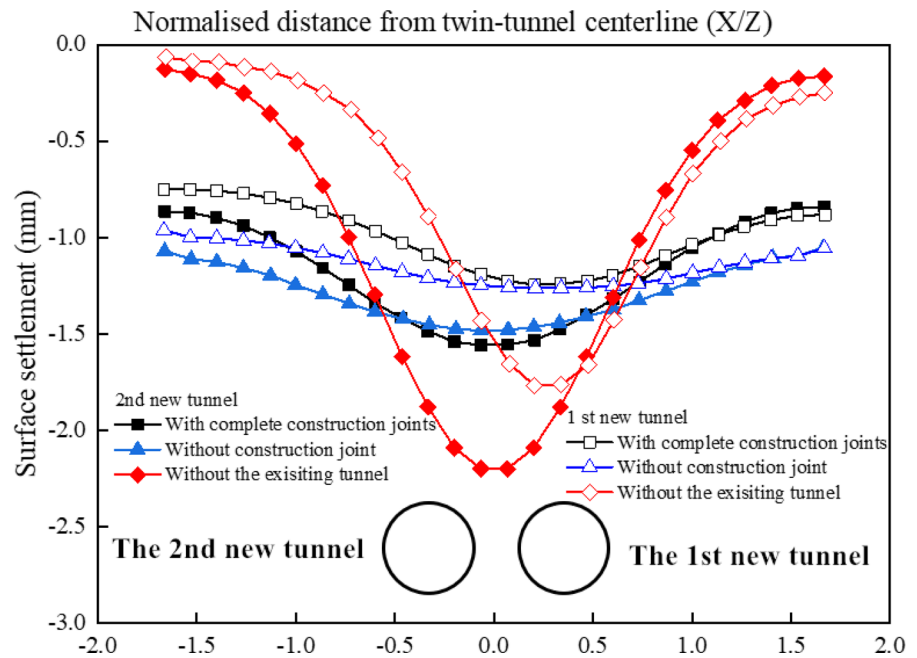
bending moment of high-speed railway tunnel lining with shield excavation, it can be seen that the bending moment of lining does not appear concentrated at the joint of deformation joints. After the completion of high-speed railway tunnel construction, the maximum lining bending moment was 124.6 kN m. After the excavation of the right line and the left line of the shield, the maximum lining bending moments were 128.1 kN m and 128.4 kN m, respectively. The comparative analysis shows that the bending moment of high-speed railway tunnel lining changes little after shield excavation, and the influence of shield excavation on high-speed railway tunnel lining was small.

5.4 Surface Subsidence Caused by Shield Excavation

Figure 15 was the surface subsidence curve caused by shield excavation in three different cases, three cases are: (a) set three subsidence joints along the high-speed railway tunnel and connect with the lining; (b) The settlement joint of the high-speed railway tunnel was not considered; (c) The influence of high-speed railway tunnel was not considered.

It can be seen from the diagram that when considering the construction joint of the existing high-speed railway tunnel, the width of the ground settlement trough was obviously larger than that without considering the construction joint. Although the depth of the ground settlement trough increases during the excavation of the right line tunnel, the research results still show that the settlement trough caused by the construction joint of the high-speed railway tunnel lining was relatively narrow but deeper than that without considering the construction joint. In addition, without considering the existing tunnel, the maximum

Fig. 15 Surface subsidence curve caused by double shield excavation



ground settlement was 2.19 mm, 49% larger than that without construction joints and 41% larger than that with construction joints.

The above results show that the existence of construction joints will reduce the shielding effect of high-speed railway tunnel on surface settlement. Nevertheless, compared with the case without existing tunnels, the existing tunnels considering construction joints have obvious shielding effect on surface settlement. When ignoring the existence of existing tunnel construction joints, it will cause large settlement trough and underestimate the maximum settlement value.

5.5 Effect of Steel Pipe Pile Reinforcement on Vertical Displacement of Existing Tunnel

According to the existing high-speed railway tunnel control specification requirements (MRPRC 2018), the maximum vertical settlement of the high-speed railway tunnel in operation should not be higher than 2 mm. Combined with Fig. 9, it can be found that the maximum settlement of the existing high-speed railway tunnel caused by the construction of the double-line shield tunnel was as high as 2.56 mm, which was beyond the maximum allowable range of the specification. This shows that the soil needs to be strengthened before the shield excavation to control

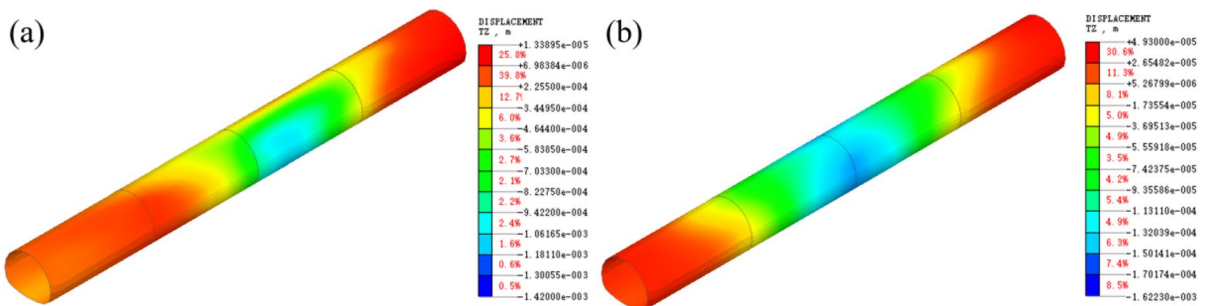


Fig. 16 Surface subsidence curve caused by double-line shield excavation **a** after excavation of 1st new tunnel; **b** after excavation of 2nd new tunnel

the settlement of the existing high-speed railway tunnel. Figure 16 was the displacement nephogram of the existing tunnel considering the reinforcement of steel pipe piles. It can be seen from the figure that the vertical displacement of the lining of the existing high-speed railway tunnel decreases significantly after the reinforcement of the steel pipe pile. When the right line tunnel construction was completed, the maximum settlement of the existing high-speed railway tunnel lining was 1.42 mm, and when the double line shield tunnel construction was completed, the maximum settlement of the existing high-speed railway tunnel lining was 1.62 mm, which was within the safe range considered in the specification. That was to ensure the safe operation of the existing high-speed railway tunnel needs to consider the reinforcement of the steel pipe pile in the shield tunnel construction.

6 Conclusion

This paper studies the influence of new shield tunnel undercrossing on existing high-speed railway tunnel. Combined with centrifuge model test and three-dimensional numerical simulation analysis results, the following conclusions can be drawn:

- (1) The trend of transverse bending strain and deformation of high-speed railway tunnel considering the settlement joint is similar to that without considering the settlement joint, but the value is slightly larger.
- (2) A refined numerical model of existing tunnels considering construction joints is proposed. The results of numerical analysis show that the construction joints of existing tunnels significantly reduce the shielding effect of existing high-speed railway tunnels on the ground. Compared with the case without considering the construction joints, the smaller shielding effect leads to the increase of the vertical displacement of the existing tunnel and the surface. When the construction joints are considered in the existing tunnel, the maximum ground settlement increases and the width of settlement trough decreases.
- (3) The settlement value of the existing tunnel caused by double-line shield tunnel construction needs to be controlled by steel pipe pile reinforcement to meet the requirements of the specification. The double-line shield tunnel construction has little effect on the internal force of the existing high-speed railway tunnel, and the reinforcement of the high-speed railway tunnel lining meets the stress requirements.
- (4) The existence of construction joints changes the mechanical response of high-speed railway tunnel structure to the construction of double-line shield tunneling. Without considering the construction joints, the numerical analysis underestimated the surface settlement, but overestimated the mechanical performance of the results of the existing tunnel.

At present, the soil was usually considered as a multi-layer uniform material, and the influence of groundwater level was usually ignored in the research process. In particular, the effective and accurate analysis in numerical simulation needs to further consider the influence of fluid–solid coupling effect on soil. The author will study it further in the future.

Acknowledgements This work was funded by the National Natural Science Foundation of China under Grant Nos. 51978669 and the China Railway Design Corporation Foundation under Grant Nos. 721239. The authors were grateful for the great support awarded.

Authors Contribution All authors contributed to the study conception and design. Material preparation, data collection and analysis were performed by LP and RF, the first draft of the manuscript was written by RF, LP, CZ, JZ and PZ. All authors commented on previous versions of the manuscript. All authors read and approved the final manuscript.

Funding This work was funded by the National Natural Science Foundation of China under Grant Nos. 51978669 and the China Railway Design Corporation Foundation under Grant Nos. 721239. The authors were grateful for the great support awarded. The authors have no relevant financial or non-financial interests to disclose.

Data Availability Enquiries about data availability should be directed to the authors.

Declarations

Conflict of interest The authors have not disclosed any competing interests.

References

- Avgerinos V, Potts DM, Standing JR (2017) Numerical investigation of the effects of tunneling on existing tunnels. *Géotechnique* 67(9):808–822. <https://doi.org/10.1680/jgeot.SiP17.P.103>
- Boonsiri I, Takemura J (2021) Observation of ground movement with existing pile groups due to tunneling in sand using centrifuge modelling. *Geotech Geol Eng* 33:621–640. <https://doi.org/10.1007/s10706-015-9845-0>
- Boonyarak T, Ng CWW (2015) Effects of construction sequence and cover depth on crossing-tunnel interaction. *Can Geotech J* 52:851–867. <https://doi.org/10.1139/cgj-2014-0235>
- Byun GW, Kim DG, Lee SD (2006) Behavior of the ground in rectangularly crossed area due to tunnel excavation under the existing tunnel. *Tunn Undergr Space Technol* 21(3):361. <https://doi.org/10.1016/j.tust.2005.12.178>
- Chakeri H, Hasanpour R, Hindistan MA, Ünver B (2011) Analysis of interaction between tunnels in soft ground by 3D numerical modeling. *B Eng Geol Environ* 70(3):439–448. <https://doi.org/10.1007/s10064-010-0333-8>
- Chen R, Meng F, Li Z, Ye Y, Ye J (2016) Investigation of response of metro tunnels due to adjacent large excavation and protective measures in soft soils. *Tunn Undergr Space Technol* 58:224–235. <https://doi.org/10.1016/j.tust.2016.06.002>
- Fang Q, Zhang D, Li Q, Wong LNY (2015) Effects of twin tunnels construction beneath existing shield-driven twin tunnels. *Tunn Undergr Space Technol* 45:128–137. <https://doi.org/10.1016/j.tust.2014.10.001>
- Gue CY, Wilcock MJ, Alhaddad MM, Elshafie MZEB, Soga K, Mair RJ (2017) Tunneling close beneath an existing tunnel in clay—perpendicular undercrossing. *Tunn Urban Environ*. <https://doi.org/10.1680/jgeot.SiP17.P.117>
- Huang Z, Zhang H, Long Z, Qiu WG, Meng GW, Zhu LC (2021) Field test optimization of shield tunnelling parameters undercrossing an existing high-speed railway tunnel: a case study. *Geotech Geol Eng* 39:1381–1398. <https://doi.org/10.1007/s10706-020-01564-3>
- Ishihara K (1993) Liquefaction and flow failure during earthquakes. *Géotechnique* 43(3):351–415. <https://doi.org/10.1680/geot.1993.43.3.351>
- Klar A, Dromy I, Linker R (2014) Monitoring tunneling induced ground displacements using distributed fiber-optic sensing. *Tunn Undergr Space Technol* 40:141–150. <https://doi.org/10.1016/j.tust.2013.09.011>
- Koukoutas SP, Sofianos AI (2015) Settlements due to single and twin tube urban EPB shield tunnelling. *Geotech Geol Eng* 33:487–510. <https://doi.org/10.1007/s10706-014-9835-7>
- Kuszyk R, Sieminska-Lewandowska A (2021) Subsidence trough asymmetry calculations in twin tube TBM tunneling. *Arch Civ Eng* 67(2):675–689. <https://doi.org/10.24425/ace.2021.137191>
- Li P, Du S, Ma X, Yin Z, Shen S (2014) Centrifuge investigation into the effect of new shield tunneling on an existing underlying large-diameter tunnel. *Tunn Undergr Space Technol* 42:59–66. <https://doi.org/10.1016/j.tust.2014.02.004>
- Liu H, Li P, Liu J (2011) Numerical investigation of underlying tunnel heave during a new tunnel construction. *Tunn Undergr Space Technol* 26:276–283. <https://doi.org/10.1016/j.tust.2010.10.002>
- Liu B, Zhang DW, Yang C, Zhang QB (2020) Long-term performance of metro tunnels induced by adjacent large deep excavation and protective measures in Nanjing silty clay. *Tunn Undergr Space Technol* 95:103147. <https://doi.org/10.1016/j.tust.2019.103147>
- MRPRC (2018) Standard for constructional quality acceptance of high speed railway track engineering (TB 10754–2018). Ministry of Railways of the People's Republic of China, China
- Ng CWW, Boonyarak T, Ma'sín D (2013) Three-dimensional centrifuge and numerical modeling of the interaction between perpendicularly crossing tunnels. *Can Geotech J* 50:935–946. <https://doi.org/10.1139/cgj-2012-0445>
- Ng CWW, Boonyarak T, Masin D (2015) Effects of pillar depth and shielding on the interaction of crossing multitunnels. *J Geotech Geoenviron* 141:04015021–04015031. [https://doi.org/10.1061/\(ASCE\)GT.1943-5606.0001293](https://doi.org/10.1061/(ASCE)GT.1943-5606.0001293)
- Ng CWW, Wang R, Boonyarak T (2016) A comparative study of the different responses of circular and horseshoe-shaped tunnels to an advancing tunnel underneath. *Geotech Lett* 6:168–175. <https://doi.org/10.1680/jgele.16.00001>
- Ng CWW, Fong KY, Liu HL (2018) The effects of existing horseshoe-shaped tunnel sizes on circular crossing tunnel interactions: three-dimensional numerical analyses. *Tunn Undergr Space Technol* 77:68–79. <https://doi.org/10.1016/j.tust.2018.03.025>
- Ng CWW, Wong YYA, Shakeel M (2022) Effects of the skew angle of new tunneling on an existing tunnel: three-dimensional centrifuge and numerical modeling. *Can Geotech J* 59:1728–1742. <https://doi.org/10.1139/cgj-2021-0413>
- Nguyen XL, Wu L, Nguyen KT et al (2021) Research on launching technology of shield tunnel in Ho Chi Minh metro line 1. *Arch Civ Eng* 67(1):387–401. <https://doi.org/10.24425/ace.2021.136479>
- Pan W, Gao Z, Zheng C, Gong Z (2018) Analysis on the influence of cross tunnel construction on the deformation of the existing high-speed railway tunnel. *Geotech Geol Eng* 36:4001–4013. <https://doi.org/10.1007/s10706-018-0553-4>
- Shi JW, Wei JQ, Ng CWW, Lu H (2019a) Stress transfer mechanisms and settlement of a floating pile due to adjacent multi-propped deep excavation in dry sand. *Comput Geotech* 116:103216. <https://doi.org/10.1016/j.compgeo.2019.103216>
- Shi JW, Fu ZZ, Guo WL (2019b) Investigation of geometric effects on three-dimensional tunnel deformation mechanisms due to basement excavation. *Comput Geotech* 106:108–116. <https://doi.org/10.1016/j.compgeo.2018.10.019>
- Wang Z, Zhang K, Wei G, Li B, Li Q, Yao W (2018) Field measurement analysis of the influence of double shield tunnel construction on reinforced bridge. *Tunn Undergr Space Technol* 81:252–264. <https://doi.org/10.1016/j.tust.2018.06.018>

- Yin M, Jiang H, Jiang Y, Sun Z, Wu Q (2018) Effect of the excavation clearance of an under-crossing shield tunnel on existing shield tunnels. *Tunn Undergr Space Technol* 78:245–258. <https://doi.org/10.1016/j.tust.2018.04.034>
- Zhang Z, Huang M (2014) Geotechnical influence on existing subway tunnels induced by multiline tunneling in Shanghai soft soil. *Comput Geotech* 56(3):121–132. <https://doi.org/10.1016/j.compgeo.2013.11.008>
- Zhang Q, Ke Wu, Cui S, Yalin Yu, Zhang Z, Zhao J (2019) Surface settlement induced by subway tunnel construction based on modified peck formula. *Geotech Geol Eng* 37:2823–2835. <https://doi.org/10.1007/s10706-018-00798-6>

Publisher's Note Springer Nature remains neutral with regard to jurisdictional claims in published maps and institutional affiliations.

Springer Nature or its licensor (e.g. a society or other partner) holds exclusive rights to this article under a publishing agreement with the author(s) or other rightsholder(s); author self-archiving of the accepted manuscript version of this article is solely governed by the terms of such publishing agreement and applicable law.